Improving Failure Analysis by Scanning Transmission Electron Diffraction Microscopy with Beam Precession

Abstract

The significance of scanning transmission electron microscopy (STEM) in failure analysis has surged since the introduction of advanced technology nodes, which have become increasingly miniaturized and more complex. Four-dimensional scanning transmission electron microscopy (4D-STEM) is an innovative electron diffraction technique that expands conventional STEM imaging and EDX mapping, enabling phase and orientation mapping of crystalline and amorphous phases in deposited thin films at nanometer resolution. Enhancing electron diffraction data with beam precession is crucial for higher accuracy and precision, particularly in the case of strain measurements. The efficacy of precession-assisted 4D-STEM analysis is illustrated through examples, such as the separation of germanium within a Ge-rich GeSbTe layer in a phase memory device. These advanced electron diffraction measurements are now accessible to a wide range of users in routine analytical procedures, thanks to unprecedented levels of automation and synchronization in the new analytical STEM instrument, TESCAN TENSOR.

Introduction

The push for faster data processing, quicker signal transmission, larger storage capacity, and lower power consumption is driving the ongoing advancement of semiconductor devices. To achieve these improvements, it's necessary to increase the density of active elements and shorten signal paths within these devices. This presents significant challenges for semiconductor manufacturers, who must accurately characterize the chemistry and morphology of specific sites on ever-smaller devices. As a result, comprehensive and complementary analytical methods are used to characterize chemical and structural properties, as well as specimen morphology, down to the nanometer scale. Analytical scanning transmission electron microscopy (STEM) has become the go-to method for quantitative characterization of semiconductor devices at the nanoscale, both for failure analysis and in process development [1, 2].

Recent breakthroughs in STEM microscope technology and high-speed direct electron detectors, with extensive dynamic range, have made it possible to perform scanning electron diffraction measurements using nanobeam illumination in the STEM mode. Here, a 2D region of interest (ROI) is scanned with an electron nanobeam just a few nanometers in diameter, capturing 2D diffraction patterns at each scanned point. Each diffraction pattern provides structural details about the crystalline or amorphous state of the sample at the corresponding pixel. These electron diffraction datasets, known as 4D-STEM datasets [3], can be utilized to determine the distribution of different phases in samples or to segment individual grains in crystalline phases based on their orientations [4, 5]. These analyses are crucial in the semiconductor industry, as the electrical performance and functionality of devices heavily depend on the type and distribution of crystalline phases in deposited layers.

Electron diffraction data are often compromised by dynamical scattering, which affects the accuracy and precision of analytical measurements. This is due to the inhomogeneous intensity of diffraction peaks, the presence of forbidden reflections, and background signals like Kikuchi lines [6, 7]. To mitigate these issues, fast beam precession is used during 4D-STEM data acquisition. This technique involves multiple cycles of beam precession for each diffraction pattern, significantly enhancing the quality of the electron diffraction datasets (Fig. 1). The improved data quality leads to greater accuracy and precision in analytical measurements, making it highly effective for semiconductor failure analysis and process development applications [8].

Over the past decade, NanoMEGAS has introduced electron beam precession as an additional module for conventional TEM/STEM electron microscopes, making it commercially available [9]. This has led to the development and implementation of numerous 4D-STEM applications within the ASTAR software package, such as phase and orientation mapping and strain analysis [10]. Despite these advancements, the widespread adoption of 4D-STEM techniques enhanced by beam precession has been somewhat limited. This is attributed to the intricate nature of experimental setups, difficulties in synchronizing microscopes, prolonged data acquisition times, and the requirement for extensive post-processing.

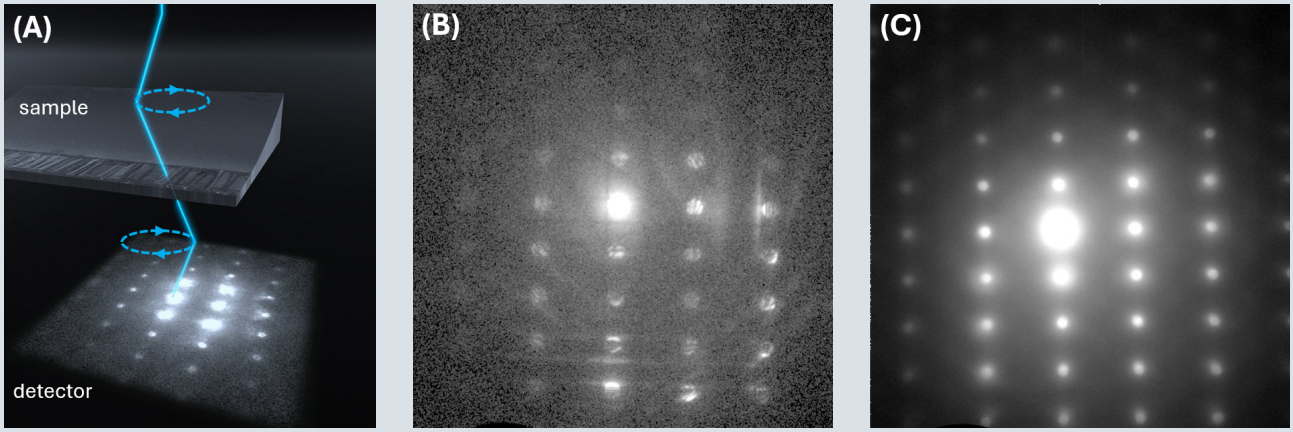

▲ **Figure 1:** Illustration of electron beam precession (blue) during the acquisition of an electron diffraction pattern from a single pixel in a 4D-STEM dataset (A). Diffraction patterns of GaN taken along the [210] zone axis, shown without beam precession (B) and with 0.8° beam precession (C).

In this presentation, we showcase a novel approach that fully integrates microscope hardware components with advanced system automation. This method facilitates the rapid acquisition and processing of precession-assisted 4D-STEM datasets with minimal user intervention, ensuring reproducibility and swift results. Diffraction data are processed in real-time, allowing for interactive analysis and visualization within the same user-friendly software environment.

Improved Failure Analysis of PCM

Phase change memory (PCM) offers several advantages for nonvolatile memory devices, including high speed, good cycling endurance, and high scalability [11]. PCM must also exhibit good SET-RESET performance and high reliability. As operating conditions of PCM are more demanding, failure analysis of PCM devices has grown increasingly important. Typically, PCM failure analysis reports either void formation or gradual segregation of elements under electric stress in the active region. The impact of material phase (incomplete crystallization) outside the active region on PCM performance has also been reported [12].

Comprehensive and complementary analytical capabilities are essential for measuring chemical and structural properties and specimen morphology down to the nanometer scale. These analyses address and quantify the typical questions in PCM failure analysis, such as: *i)* How does the grain structure and/or compositional map vary in the two switched states? *ii)* How do process deposition variables affect the film structure? *iii)* How does the grain structure (size, orientation, defects) change when the device is annealed at different production steps?

Material and Methods

The PCM device used in this study was provided by STMicroelectronics, Grenoble, France. The TEM lamella was prepared by FIB milling, lift-out, and polishing.

Bright-field (BF) and annular dark field (ADF) STEM images were acquired with a convergence semi-angle of 10 mrad, a probe current of 100 pA, and a dwell time of 5 µs. EDX maps were acquired with a 4 nA probe current and a total acquisition time of 600 s. Diffraction patterns were acquired using precession-assisted 4D-STEM with a probe convergence semi-angle of 2 mrad, a 50 pA probe current, a precession angle of 0.8°, and a dwell time of 2 ms (500 frames per second). The total data acquisition time was approximately 5 minutes.

Phase and orientation maps were determined by comparing and matching each diffraction pattern in the collected 4D-STEM dataset with a set of precalculated kinematical templates that were generated using known crystalline structures (published crystal information files, CIF) or measured directly from the sample for different amorphous phases (scattering rings in diffraction patterns). For each pixel of the map, the best matching template was identified using a cross-correlation-based scoring function and the phase and orientation were assigned accordingly [10]. In total, five crystalline phases and three different amorphous phases were fitted simultaneously in this case. Data processing on a standard workstation took approximately 15 minutes.

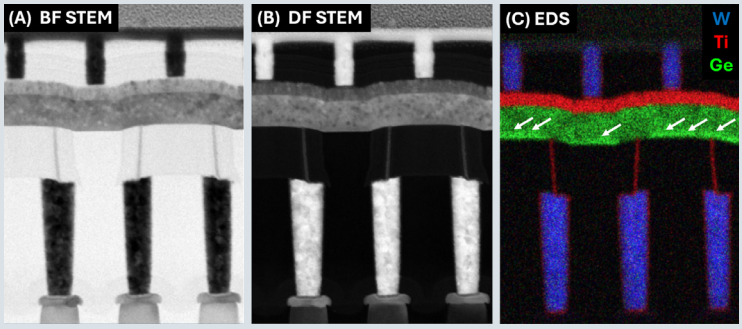

Figure 2: Bright-field (A) and dark-field (B) STEM images of the analyzed PCM device. EDX elemental map (C) of the same area highlighting regions with increased concentration of Ge in the GST layer (indicated by arrows).

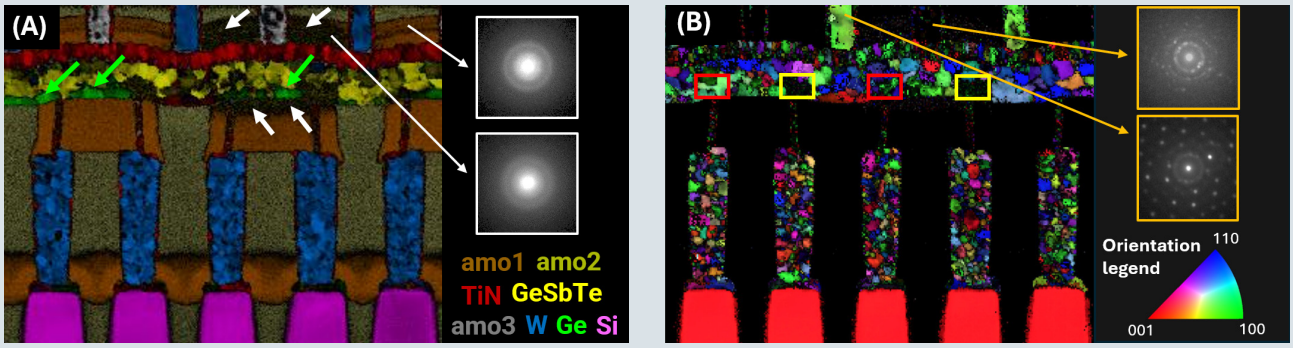

Figure 3: (A) 4D-STEM phase map of the PCM, showing several crystalline and amorphous phases. Germanium segregates from the GST layer at the bottom interface (green arrows). The phase map is overlaid with a greyscale phase reliability map, revealing areas with low template matching reliability (white arrows) due to altered diffraction of the amo1 phase (right). (B) 4D-STEM orientation map of the PCM, showing individual grains in the crystalline phases, segmented by their z-orientation (legend). Red and yellow rectangles indicate positions in the GST layer corresponding to the SET and RESET states of the PCM, respectively. Diffraction patterns of different tungsten states in PCM vias are also shown (right).

Results

The architecture of the PCM core structure, including GeSbTe (GST) and TiN thin layers, tungsten vias and contacts, was revealed by conventional dark field STEM imaging and EDX elemental mapping (Fig. 2). The EDX elemental map showed that the GST layer exhibited inhomogeneous distribution of germanium at the bottom interface of the GST layer.

To gain more insight into the segregation of elements and phase distributions within the GST and TiN layers, precession-assisted 4D-STEM was used. This technique distinguishes different elements and compounds based on their crystal structure and orientation of individual grains in the map.

The 4D-STEM phase map in Figure 3A reveals the segregation of crystalline germanium at the bottom interface of the GST layer, where it connects to the PCM heater (indicated by green arrows). This phase map is overlaid with a greyscale reliability map, to indicate the uniqueness of the template matching. Darker regions within the crystalline and amorphous phase maps indicate areas with lower reliability. The white arrows highlight regions in the amorphous layer (amo1) above the TiN layer and below the GST layer. Decreased phase reliability scores and diffraction data suggest alterations in the amo1 phase in these regions, as evidenced by different amorphous diffraction patterns in Figure 3A. Tungsten in PCM vias was found in two different states, one corresponding to a tungsten crystal (blue) and the other close to an amorphous state (grey).

The 4D-STEM orientation map (Fig. 3B) displays individual grains of the crystalline phases based on their different orientations in the sample. The states of tungsten in the PCM vias are clearly distinguished as alternating single-crystal and poly-crystalline states, confirmed by representative diffraction patterns (Fig. 3B).

In Figure 3B, the GST layer exhibits regions without crystalline grains (yellow rectangles), indicating amorphous states corresponding to the RESET states. The amorphous state is confirmed in a virtual dark field STEM image (Fig. 4), constructed using a virtual mask (ring) corresponding to one scattering ring of an amorphous phase. The GST layer amorphization (RESET states) corresponds to the brighter patches above the heater contacts (blue arrows), as evidenced by a diffraction pattern of diffuse scattering rings without diffraction spots (bottom right). These amorphous regions also exhibit lower phase reliability in Figure 3A.

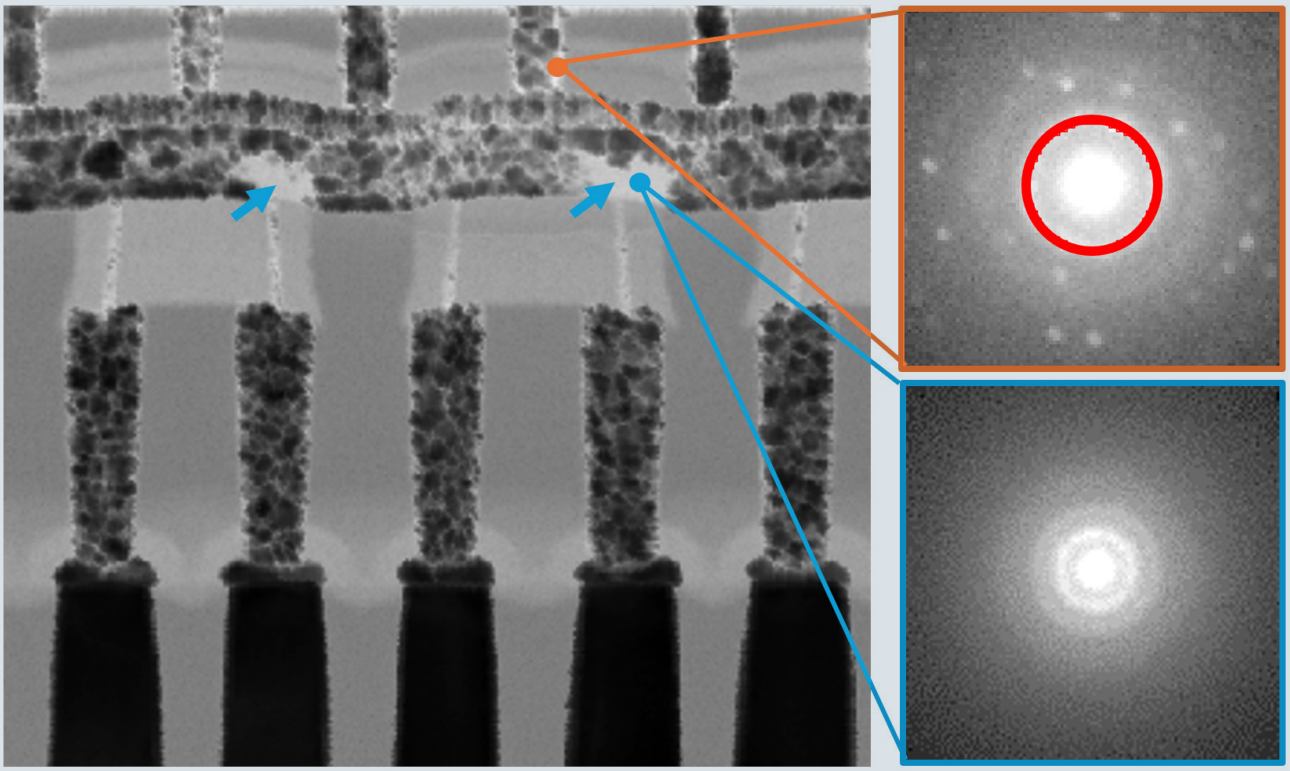

▲ Figure 4: Virtual dark field STEM image (left) constructed using a virtual mask (red circle circumference), shown in a representative diffraction pattern with diffuse scattering rings from an amorphous phase, alongside diffraction spots from small grains in the vias (top right). The GST layer amorphization (RESET states) appears as brighter patches (blue arrows), where diffraction patterns exhibit only diffuse scattering rings without diffraction spots (bottom right).

Conclusions

Using precession-assisted 4D-STEM for phase and orientation mapping of a GST layer in a PCM device, we successfully identified and validated the suspected segregation of germanium from the GST layer. The phase map also revealed an altered conformation of one amorphous layer at a specific location in the device, possibly due to failure of a specific heater segment. Additionally, the orientation map showed crystallization and localized amorphization in the GST layer, corresponding to SET and RESET states at the position of contacts from the heater side of the device.

The optimization of the TESCAN TENSOR design for electron diffraction, enhanced by fast and accurate beam precession, has enabled rapid and interactive characterization of semiconductor devices. Beyond conventional STEM imaging and EDS mapping, 4D-STEM phase and orientation mapping can now be performed regularly with minimal difficulty, and the integrated beam precession improves data quality while accuracy [13]. In the PCM-device characterization example, all diffraction data and results were obtained within 15 minutes, which is over ten times faster than using conventional STEM instruments with beam precession modules.

Acknowledgments

We are grateful to STMicroelectronics (Grenoble, France) for providing the semiconductor device used in this multimodal phase and orientation analysis study. We especially want to thank Pascal Gounet (STMicroelectronics, Grenoble, France) and Francesco Cazzaniga (STMicroelectronics, Agrate, Italy) for their valuable discussions throughout the course of this work.

References

1. R.S. Rai and S. Subramanian, "Role of transmission electron microscopy in the semiconductor industry for process development and failure analysis," *Progress in Crystal Growth and Characterization of Materials, Vol. 55 (2009), p 63-97. doi:10.1016/j.pcrysgrow.2009.09.002*

2. *M. de la Mata M and S.I. Molina, "STEM Tools for Semiconductor Characterization: Beyond High-Resolution Imaging," Nanomaterials (Basel), Vol. 12, No. 3 (2022), p 337. doi:10.3390/nano12030337*

3. C. Ophus, "Four-Dimensional Scanning Transmission Electron Microscopy (4D-STEM): From Scanning Nanodiffraction to Ptychography and Beyond," *Microsc Microanal.*, Vol. 25, No. 3 (2019), p 563-582. doi:10.1017/S1431927619000497

4. E.F. Rauch and M. Veron, "Coupled microstructural observations and local texture measurements with an automated crystallographic orientation mapping tool attached to a TEM," *J. Mater. Sci. Eng. Tech., Vol. 36, No. 10 (2005), p 552-556. doi:10.1002/mawe.200500923*

5. E.F. Rauch, *et al., "New Features in Crystal Orientation and Phase Mapping for Transmission Electron Microscopy," Symmetry, Vol. 13 (2021), p 1675. doi:10.3390/sym13091675*

6. *A.S. Eggeman and P.A. Midgley, Advances in Imaging and Electron Physics, Vol. 170, Elsevier Inc. (2012), p 1-63. doi:10.1016/B978-0-12-394396-5.00001-4.*

7. *P. Oleynikov, et al., "Precession electron diffraction: Observed and calculated intensities," Ultramicroscopy, Vol. 107, No. 6-7 (2007), p 523-533. doi:10.1016/j.ultramic.2006.04.032*

8. *P.A. Midgley, A.S. Eggeman, "Precession electron diffraction - a topical review," IUCrJ, Vol. 2, No. 2 (2015), p 126-136. doi:10.1107/S2052252514022283*

9. *A. Avilov, et al., "Precession technique and electron diffractometry as new tools for crystal structure analysis and chemical bonding determination," Ultramicroscopy, Vol. 107, No. 6-7 (2007), p 431-444.*

10. *A.D. Darbal, et al., "Nanoscale Automated Phase and Orientation Mapping in the TEM", Microscopy Today, Vol. 20, No. 6 (2012), p 38-42. doi:10.1017/S1551929512000818*

11. G. W. Burr, *et al.*, "Phase change memory technology," *J. Vac. Sci. Technol. B*, Vol. 28, No. 2 (2010) p 223-262. doi:10.1116/1.3301579.

12. Y. Wang, *et al.*, "Failure Analysis and Performance Improvement of Phase Change Memory Based on $Ge_2Sb_2Te_5$," *IEEE Trans. Device Mater. Reliab.*, Vol. 21, No. 2 (2021), p 236-239, doi:10.1109/TDMR.2021.3065217

13. D. van der Wal, "Scanning Transmission Electron Microscopy Done Right," *Microscopy Today*, Vol. 31, No. 2 (2023), p 15–17. doi:10.1093/mictod/qaad009

TESCAN GROUP, a.s.
Libušina tř. 21, 623 00 Brno - Kohoutovice / Czech Republic
(phone) +420 530 353 411 / (email) sales@tescan.com / marketing@tescan.com

TESCAN